Materials Horizons

COMMUNICATION

View Article Online
View Journal | View Issue

Cite this: *Mater. Horiz.*, 2016, 3, 613

Received 29th July 2016,
Accepted 7th October 2016

DOI: 10.1039/c6mh00275g

www.rsc.li/materials-horizons

Optical phonons in methylammonium lead halide perovskites and implications for charge transport†

Michael Sendner,[ab] Pabitra K. Nayak,[c] David A. Egger,[d] Sebastian Beck,[ab] Christian Müller,[abe] Bernd Epding,[ae] Wolfgang Kowalsky,[abe] Leeor Kronik,[d] Henry J. Snaith,[c] Annemarie Pucci[abf] and Robert Lovrinčić*[ae]

Lead-halide perovskites are promising materials for opto-electronic applications. Recent reports indicated that their mechanical and electronic properties are strongly affected by the lattice vibrations. Herein we report far-infrared spectroscopy measurements of $CH_3NH_3Pb(I/Br/Cl)_3$ thin films and single crystals at room temperature and a detailed quantitative analysis of the spectra. We find strong broadening and anharmonicity of the lattice vibrations for all three halide perovskites, which indicates dynamic disorder of the lead-halide cage at room temperature. We determine the frequencies of the transversal and longitudinal optical phonons, and use them to calculate, *via* appropriate models, the static dielectric constants, polaron masses, electron–phonon coupling constants, and upper limits for the phonon-scattering limited charge carrier mobilities. Within the limitations of the model used, we can place an upper limit of 200 $cm^2\ V^{-1}\ s^{-1}$ for the room temperature charge carrier mobility in $MAPbI_3$ single crystals. Our findings are important for the basic understanding of charge transport processes and mechanical properties in metal halide perovskites.

Conceptual insights

Metal halide perovskites are an outstanding material class for opto-electronics. The interplay of electronic and structural dynamics in these materials is currently under scrutiny. One of the open questions is the nature of electron–phonon interactions, which may bear important implications for charge-carrier generation and transport. We report here a detailed quantitative analysis of far-infrared spectra of the three methylammonium lead halide perovskites ($CH_3NH_3Pb(I/Br/Cl)_3$). This allows us to deduce electron–phonon coupling constants and polaron masses, which are consistent with a large polaron picture for the free charges. Using the Feynman model in conjunction with our data, we set an upper limit for the optical phonon limited charge carrier mobilities at room temperature of $\sim$200 $cm^2\ V^{-1}\ s^{-1}$ for $CH_3NH_3PbI_3$. Our findings help to understand fundamental electrical transport mechanisms in metal halide perovskites.

1 Introduction

Lead-halide perovskites, with the general chemical structure ABX_3, have recently reemerged as promising materials for opto-electronic applications.[1–3] The most prominent candidates to date for perovskite-based solar cells are the hybrid organic–inorganic perovskites ABX_3,[4] where A is the organic cation, B = Pb, and X is the halide. The most widely studied examples in this material class are the methylammonium (MA) lead halides[5] ($MAPb(I/Br/Cl)_3$). Their bandgaps range from approximately 1.6 eV ($MAPbI_3$) to 3.0 eV ($MAPbCl_3$).[6] They exhibit structural phase transitions in an orthorhombic–tetragonal–cubic sequence, with $MAPbI_3$ being tetragonal at room temperature, and $MAPbBr_3$ and $MAPbCl_3$ being both cubic.[7] As these phase transitions can occur close to room temperature, structural fluctuations of the lead-halide cage have potentially strong impact on the opto-electronic properties.[8]

Long charge carrier diffusion lengths exceeding 1 μm have been reported for $MAPbI_3$ and $MAPbBr_3$ single crystals and thin films.[9–11] The Urbach energies in these materials are $\sim$15 meV, comparable to the values for typical inorganic crystalline semiconductor materials like GaAs,[12] suggesting a low prevalence of bandgap states, which often lower the carrier mobilities in semiconductors. Despite the low number of band gap states and the often observed high structural order of the corner sharing lead halide octahedras, the charge carrier mobilities are modest, especially in view of the low effective masses.[13,14] Moreover, the thermal conductivity of $MAPbI_3$ has recently been calculated to be ultralow.[15] All of these properties are intimately connected to the nature of the lattice vibrations in

[a] *InnovationLab, Speyerer Str. 4, 69115 Heidelberg, Germany*
[b] *Kirchhoff Institute for Physics, Heidelberg University, Im Neuenheimer Feld 227, 69120 Heidelberg, Germany*
[c] *Clarendon Laboratory, Department of Physics, University of Oxford, Oxford OX1 3PU, UK*
[d] *Department of Materials and Interfaces, Weizmann Institute of Science, Rehovoth 76100, Israel*
[e] *Institute for High Frequency Technology, TU Braunschweig, Schleinizstr. 22, 38106 Braunschweig, Germany. E-mail: r.lovrincic@tu-braunschweig.de*
[f] *Centre for Advanced Materials, Heidelberg University, Germany*
† Electronic supplementary information (ESI) available. See DOI: 10.1039/c6mh00275g

these materials. In particular, the modest charge carrier mobilities have been explained by either predominant electron scattering from acoustic[16–19] or optical phonons[20–22] or the formation of polarons.[19,23–26] Furthermore, recently the influence of spin–orbit coupling on the temperature dependence of the mobility was shown theoretically.[27] To better understand such fundamental material properties, detailed knowledge of the phonon spectra is mandatory. Such can in principle be obtained from Raman measurements, which for $MAPbX_3$ are, however, experimentally challenging due to the ease of beam damage under laser irradiation. Far infrared (IR) spectroscopy circumvents the beam damage problem and reveals information complementary to Raman spectroscopy. Several far-IR studies of $MAPbX_3$ have appeared over the last two years.[20,28,29] Pérez-Osorio *et al.* measured the frequency of the transversal optical (TO) phonons and theoretically predicted a strong LO–TO splitting for the strongest vibration.[29] Wright *et al.* estimated the longitudinal optical (LO) phonon frequencies indirectly *via* temperature dependent photoluminescence measurements (ω_{LO} = 11.5 and 15.3 meV, 92 and 122 cm^{-1}).[22] However, a direct experimental determination of the LO phonon frequency is currently missing. In view of the fact that LO phonons can interact with charge carriers, it is important to understand charge transport close to room temperature.

Herein we report far-IR spectra of the three methylammonium lead halide perovskite ($MAPb(I/Br/Cl)_3$) thin films and provide a detailed quantitative analysis of the lattice vibrations corroborated by reflectance measurements on single crystals. From these data, we determine the frequencies and damping coefficients of both LO and TO phonons and find strong broadening and anharmonicity of the lattice vibrations for all three halide perovskites. This indicates dynamic disorder of the lead-halide cage at room temperature, in agreement with recent low frequency, off-resonance Raman measurements of $MAPbBr_3$.[8] From our data we calculate the static dielectric constants of all three halide perovskites *via* the Cochran-Cowley relation.[30] We use the derived dielectric constants and phonon frequencies to estimate electron–phonon coupling constants and polaron masses. To quantify the importance of optical vibrations for charge transport, we employ the Feynman polaron model at elevated temperatures in conjunction with exciton effective masses, which provides upper limits for the optical phonon-scattering limited charge carrier mobilities in methylammonium lead halide perovskites.

2 Results

We measured far IR spectra in the range of 30–300 cm^{-1}, which contain information on the Pb–X lattice vibrations, in contrast to the mid IR range that is dominated by molecular vibrations of the MA cation.[31–33] Fig. 1 compares measurements of a $MAPbI_3$ thin film under two angles of incidence with the measurement of the corresponding lead halide, PbI_2. Whereas at normal incidence one can only determine the resonance frequency of the TO mode (ω_{TO}), it is possible to additionally determine the position of the longitudinal optical vibration (ω_{LO}) at non-normal incidence *via* the Berreman mode.[34] For polar materials such as $MAPbI_3$ the LO frequency is higher than the TO frequency, hence a clear LO–TO splitting occurs. The peak positions for $MAPbI_3$ and PbI_2, determined through detailed analysis of the data as discussed below, are indicated in Fig. 1 and differ by only ~10 cm^{-1}. This is reasonable given the similar bulk moduli B for the two materials,[35] which are directly related to the LO frequency of the crystals ($B \propto \omega_{LO}^2$).[36] The strong broadening and asymmetry of the main TO mode of $MAPbI_3$ at 63 cm^{-1} (8 meV) is apparent when compared to the sharp and symmetric TO mode of PbI_2. Since $MAPbI_3$ is highly crystalline, as evidenced by typically very sharp XRD peaks at room temperature, the phonon broadening is unlikely to be explained by static disorder caused by the micro strain present in polycrystalline thin films, because the broadening is also present in single crystals as we show below. We rather attribute it to dynamic disorder of the perovskite structure,[8,37–40] similar to certain oxide perovskites.[41] Given the frequency range of our measurements and the similar peak positions of $MAPbI_3$ and PbI_2, this likely originates from disorder of the lead-halide framework that is coupled to fast reorientations of the methylammonium cation,[31,42] and possibly accompanied by strongly anharmonic hopping of Pb and/or I.[8,43]

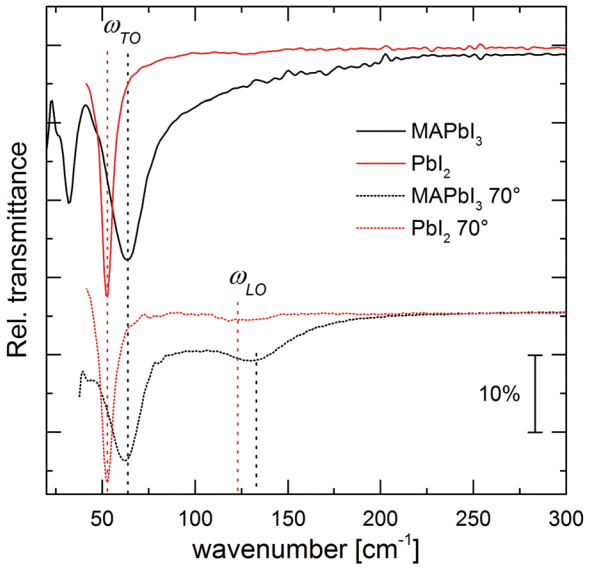

Fig. 1 Relative transmittance of a 266 nm thick $MAPbI_3$ (black) and a 130 nm thick PbI_2 (red) thin film on a silicon substrate under normal incidence (solid), and under 70° angle of incidence (dashed) with unpolarized light. The positions of the strongest respective TO and LO modes are marked with dashed vertical lines.

Fig. 2 shows the measured far IR spectra of all three methylammonium lead halides at two angles of incidence, together with optically modeled spectra. Given the strong LO–TO splitting and anharmonic phonon coupling apparent in our data, a harmonic potential of the vibrations cannot be assumed anymore. Therefore, we use the Gervais model[43] to fit the spectra for the dielectric function, which extends the harmonic oscillator model to the case of strong oscillations and, in contrast to a

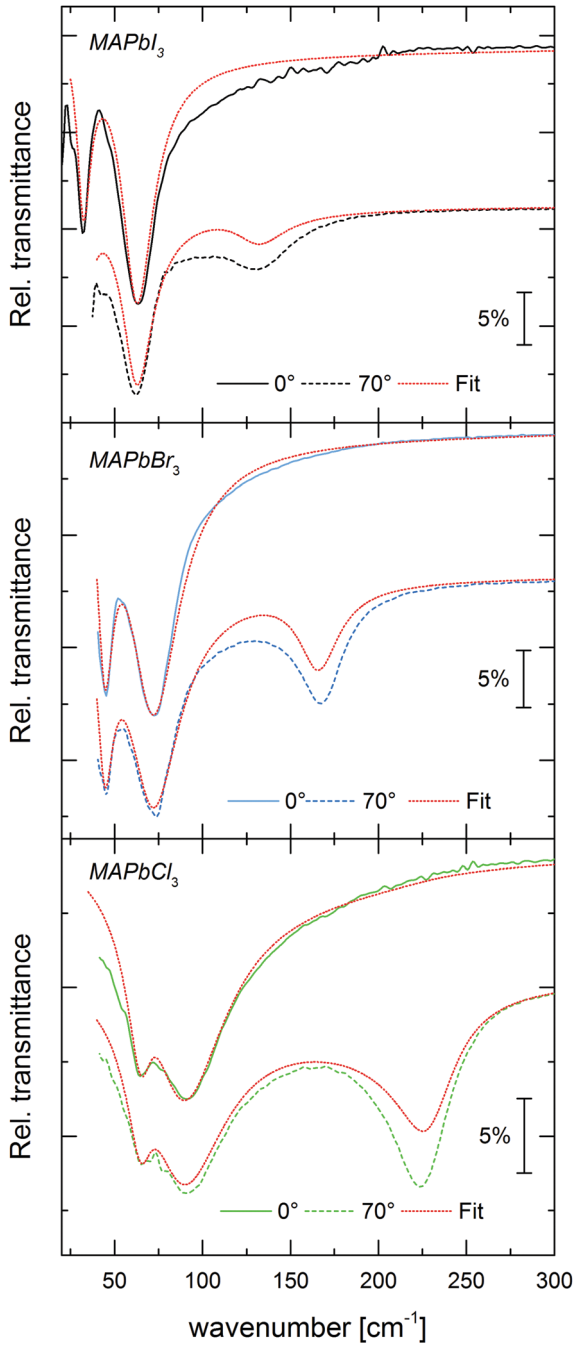

Fig. 2 Relative transmittance of 266 nm thick $MAPbI_3$ (black), 287 nm thick $MAPbBr_3$ (blue) and 226 nm thick $MAPbCl_3$ (green) thin films on silicon substrates at normal incidence (solid) and at 70° angle of incidence (dashed) with unpolarized light. Model fits for both angles of incidence for every $MAPbX_3$, are shown in red dashed lines, with the resulting dielectric function shown in Fig. 4.

Lorentz oscillator, allows for different damping coefficients for LO and TO phonons (γ_{LO}, γ_{TO}):[43,44]

$$\varepsilon(\omega) = \varepsilon_\infty \prod_n \frac{\omega_{LO,n}{}^2 - \omega^2 + i\gamma_{LO,n}\omega}{\omega_{TO,n}{}^2 - \omega^2 + i\gamma_{TO,n}\omega}. \quad (1)$$

The model takes into account that TO modes appear as the poles of $\varepsilon(\omega)$, and LO modes as the zeros of $\varepsilon(\omega)$.[43] The high frequency dielectric background ε_∞ is taken from mid-infrared spectral modeling.[32] Two oscillators were used in eqn (1) to model the spectra for each thin film, simultaneously for the two angles of incidence – one rather strong oscillator and a second weaker one on the low energy side of the spectrum. Although the fits show minor deviations from the measured data, the agreement is very good overall. Following previously published theoretical calculations,[29] we assign the mode at 32 cm^{-1} in $MAPbI_3$ mostly to a Pb–I–Pb rocking vibration, and the stronger mode at 63 cm^{-1} mostly to a Pb–I stretching vibration. A similar assignment of modes can be assumed for $MAPbBr_3$ and $MAPbCl_3$, given their chemical similarity to $MAPbI_3$.

We performed additional far IR measurements on single crystals to corroborate the thin film results and exclude possible influence of grain boundaries. We note that due to their thickness and extinction coefficients these have to be measured in reflection geometry and that the spectra of the I and Br single crystals were scaled in intensity because the crystal facets were smaller than the IR beam diameter. Fig. 3 shows the measured reflection spectra of the single crystals together with simulated spectra that were calculated using the corresponding dielectric functions obtained from the thin film transmission measurements. All three halide perovskites display an increased reflectivity in the spectral range between the TO and LO modes. This so called Reststrahlen band is typical for polar materials with strong LO–TO splitting.[44,45] Due to the increasing ω_{TO} and ω_{LO} values from I to Cl, also the Reststrahlen band is blueshifted, as can be seen in the single crystal measurements. Importantly, we observe very good agreement between the measurements and

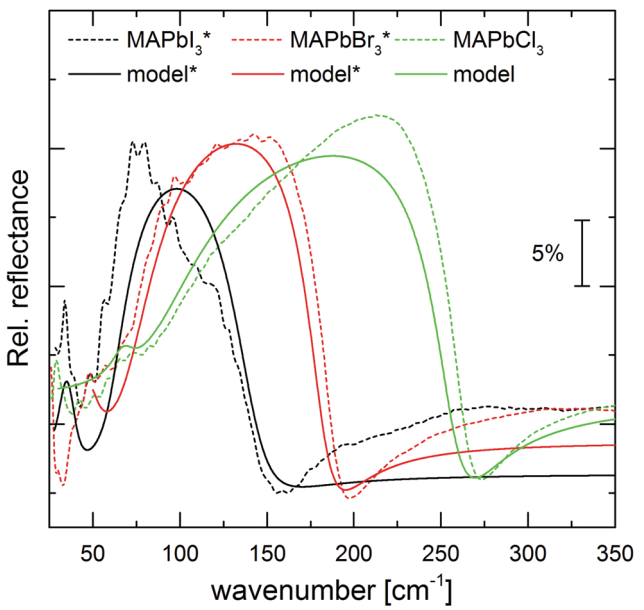

Fig. 3 Relative reflectance spectra of $MAPbI_3$ (black), $MAPbBr_3$ (red), and $MAPbCl_3$ (green) single crystals at room temperature with unpolarized light under an 80° angle of incidence (gold mirror as reference). The corresponding solid lines show calculated reflectance spectra using the dielectric function, derived for the thin films shown in Fig. 4 (spectra with star were scaled in intensity).

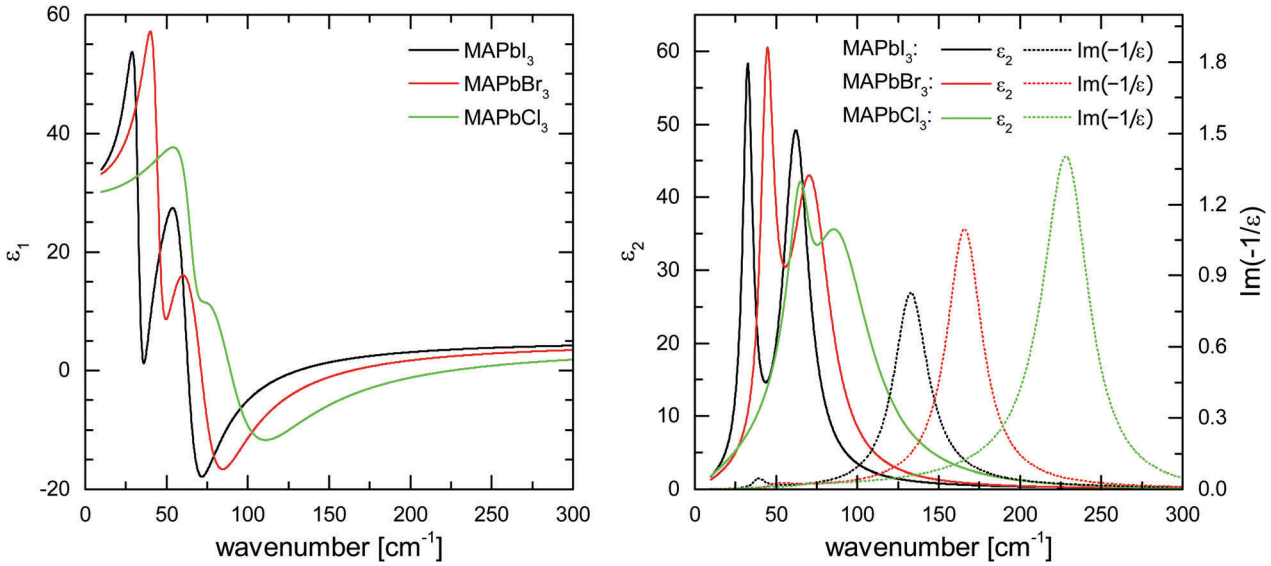

Fig. 4 Derived dielectric functions for $MAPbI_3$ (black), $MAPbBr_3$ (red) and $MAPbCl_3$ (green). Left: Real part ε_1 of the dielectric function. Right: Imaginary part ε_2 together with the loss function $\mathrm{Im}(-1/\varepsilon(\omega))$ (dashed lines). Peaks in ε_2 indicate positions of TO phonons, peaks in $\mathrm{Im}(-1/\varepsilon(\omega))$ positions of LO phonons.

calculations for all three spectra, which underlines that the dielectric functions obtained from the thin film measurements are meaningful.

The derived dielectric functions are shown in Fig. 4. The increase of the phonon frequencies in the I–Br–Cl series can be well described by the decrease of the effective ionic masses, μ_X, of halides X involved in Pb–X oscillations ($\omega_{TO} \propto \mu^{-0.5}$; $\mu_I^{-0.5} : \mu_{Br}^{-0.5} : \mu_{Cl}^{-0.5} = 1 : 1.16 : 1.61$), which strongly corroborates our assignment of these modes to lead-halide stretch vibrations. Fig. 4 also shows the loss function, $\mathrm{Im}(-1/\varepsilon(\omega))$, the peaks of which mark the positions of frequencies corresponding to LO phonons.[34]

Table 1 summarizes the determined ω_{TO} and ω_{LO} frequencies for the different halide perovskites. Using the Cochran-Cowley relation,[30]

$$\frac{\varepsilon_{Static}}{\varepsilon_\infty} = \prod_n \frac{{\omega_{LO,n}}^2}{{\omega_{TO,n}}^2}, \quad (2)$$

we calculate the static dielectric constants for the different halide perovskites, also listed in Table 1. Our derived values (33.5, 32.3, 29.8 for $MAPb(I/Br/Cl)_3$, respectively) are close to those published by Poglitsch and Weber[46] (30.5, 39, and 26 respectively; measured at $f = 90$ GHz). We note, however, that Onoda-Yamamuro *et al.* determined considerably higher values (45, 60, 58; measured at $f = 1$ kHz).[47] The discrepancy could be related to mobile ionic species that can strongly influence impedance measurements.[48]

Table 1 Summary of the obtained TO and LO phonon frequencies and dampings, as well as the high and low frequency dielectric constants

	ω_{TO} [cm^{-1}]	γ_{TO} [cm^{-1}]	ω_{LO} [cm^{-1}]	γ_{LO} [cm^{-1}]	ε_∞	ε_{Static}
$MAPbI_3$	32	9	40	11	5.0	33.5
	63	20	133	30		
$MAPbBr_3$	45	10	51	15	4.7	32.3
	73	30	167	27		
$MAPbCl_3$	66	15	70	16	4.0	29.8
	89	52	225	34		

We now examine the implications of our results for electron–phonon interactions and charge transport. Fröhlich described the movement of electrons in fields of polar lattice vibrations theoretically, introducing an interaction parameter[49,50]

$$\alpha = \frac{1}{\varepsilon^*}\sqrt{\frac{R_y}{ch\omega_{LO}}}\sqrt{\frac{m^*}{m_e}}. \quad (3)$$

The coupling constant α quantifies the interaction between a charge carrier with an effective mass m^*, and an optical phonon with frequency ω_{LO} (in [cm^{-1}] units). The ionic screening parameter, $1/\varepsilon^* = 1/\varepsilon_\infty - 1/\varepsilon_{Static}$, is used to describe an effective dielectric background. h is Planck's constant, c is the speed of light, and R_y the Rydberg energy. With multiple LO phonon branches, as is the case for the $MAPbX_3$ studied here (see Table 1), an effective ω_{LO} can be used, that is an average of the actual frequencies weighted by their spectral weight.[51] We note that this is also reasonable given the possibly strong anharmonicity of modes we find in our data, which may result in more complex scattering processes rather than interaction of carriers with discrete optical modes.

Within Fröhlich's polaron theory, as extended by Feynman, the effective mass of the polaron m_p can be calculated as[52]

$$m_p = m^*\left(1 + \frac{\alpha}{6} + \frac{\alpha^2}{40} + \ldots\right). \quad (4)$$

This means the polaron mass is higher than the effective mass obtained from band structure calculations due to electron–phonon interactions, thereby limiting the charge carrier mobility. We used $m^* = m^*_{ex}$, with m^*_{ex} being the reduced exciton mass obtained from high quality magneto-optical measurements of

Table 2 Determined polaron parameters and LO phonon scattering limited charge carrier mobilities at room temperature for the three halide perovskites (this work) and GaAs for comparison

	Effective mass[a] m^*_{ex}/m_0	Ionic screening $1/\varepsilon^*$	Coupling constant α	Polaron mass m_P/m^*_{ex}	Polaron radius l_p [Å]	Mobility μ [$cm^2\ V^{-1}\ s^{-1}$]
$MAPbI_3$	0.104[53]	0.17	1.72	1.36	51	197
$MAPbBr_3$	0.117[53]	0.18	1.69	1.35	43	158
$MAPbCl_3$	0.20	0.22	2.17	1.48	27	58
GaAs[57]	0.067	0.016	0.068	1.01	40	7000

[a] In units of the free electron mass m_0.

$MAPbI_3$ and $MAPbBr_3$.[53] For $MAPbCl_3$, we performed density functional theory (DFT) based band-structure calculations using the VASP code,[54] the PBE exchange–correlation functional[55] and accounting for spin–orbit coupling (see Methods for details). We note that the reduced exciton effective mass obtained in this way is in good agreement with recent GW calculations,[56] but individual electron and hole masses deviate more significantly. Our calculated polaron masses, as well as the coupling constants α, the ionic screening parameters $1/\varepsilon^*$, and the corresponding polaron radii

$$l_p = \sqrt{\frac{h}{2cm^*_{ex}\omega_{LO}}} \quad (5)$$

are listed in Table 2.

Importantly, these parameters can be used to estimate an upper limit for charge carrier mobilities μ in hybrid perovskites under the assumption that carriers are interacting only with optical phonons. Previously, Kadanoff's equation[58] for weakly coupled polarons in the low temperature regime was used to estimate the charge carrier mobility in $MAPbI_3$.[20] In view of the rather low Debye temperatures of $MAPbX_3$[59] and that for solar cell devices we are especially interested in μ at room temperature, we have to use the general result of Feynman *et al.*,[52,60] obtained in the absence of the low temperature approximation:[49]

$$\mu = \frac{3\sqrt{\pi}e}{2\pi c\omega_{LO}m^*_{ex}\alpha}\frac{\sinh(\beta/2)}{\beta^{5/2}}\frac{w^3}{v^3}\frac{1}{K}. \quad (6)$$

Here, $\beta = hc\omega_{LO}/k_BT$, v, and w are temperature-dependent variational parameters, and K is a function of β, v and w.[49] We calculated v and w by minimizing the free polaron energy (see ESI† for details).[49] The obtained upper limits for the charge carrier mobilities at room temperature are listed in Table 2. We find values around 200, 150, and 50 $cm^2\ V^{-1}\ s^{-1}$ for $MAPbI_3$, $MAPbBr_3$, and $MAPbCl_3$, respectively. We estimate the error bar due to experimental uncertainties in the determination of the phonon frequencies as $\pm 30\ cm^2\ V^{-1}\ s^{-1}$. The lower value for $MAPbCl_3$ is mainly a result of the higher m^*_{ex}, which is related to the higher ionicity of the Pb–Cl bonds indicated by the higher LO–TO splitting.

3 Discussion

The observed strong broadening and anharmonicity of the lattice vibrations imply a large dynamic disorder in methylammonium lead halides at room temperature. The fast reorientation of the methylammonium cation in the PbI_3 host framework certainly contributes to this dynamic disorder.[31,42,61,62] Moreover, it was recently reported that dynamic disorder is intrinsic to the general lead-halide perovskite structure even in the absence of organic cations.[8] This effect may well contribute to the broadening of the vibrations observed here. We note that the addition of a central peak to the dielectric function that would indicate strongly anharmonic hopping[41] of Pb or I, while consistent with our data, improves the quality of our fits only to a limited extent (see ESI†). Our obtained TO positions for $MAPbI_3$ are very similar to those previously published by La-o-vorakiat *et al.*[20] However, our oscillator strengths are roughly twice as large, possibly due to only partial surface coverage of the films used by La-o-vorakiat *et al.* (see ESI† for detailed comparison). We also find good qualitative agreement with a recently published dielectric function of $MAPbI_3$ obtained from DFT and MD calculations.[56] Our LO frequencies for $MAPbI_3$ and $MAPbBr_3$ are somewhat higher but still close to those indirectly estimated from temperature dependent photoluminescence measurements by Wright *et al.*,[22] confirming their analysis.

The determined polaron coupling constants for $MAPbX_3$ of $\alpha \sim 2$ are at the higher end of the range typical for weak coupling (large polarons). Nevertheless, the polaron radii are consistent with large polarons, as they are far above the lattice constants of the materials and, in fact, show that polarons are spread over several unit cells. Consequently, the polaron masses are less than 50% higher than the reduced excitonic mass determined from magneto optical studies.[53] Similar values are found by phonon calculations of $MAPbI_3$ leading to a coupling constant of 2.4 in the large polaron regime.[28,39]

A comparison of our mobility estimations to literature reports is complicated by the wide spread of published values. For example, for $MAPbI_3$ measured mobilities around 50 $cm^2\ V^{-1}\ s^{-1}$ for thin films[7,63] and 2.5 or 165 $cm^2\ V^{-1}\ s^{-1}$ for single crystals[9,64] have been reported. Overall, our estimates are at the higher end of reported values, which is what one would expect as our numbers are upper limits in the complete absence of defect scattering, acoustic phonon scattering, and the possible impact of local polaronic distortions.[24] Our findings nevertheless imply that room temperature mobilities well below 100 $cm^2\ V^{-1}\ s^{-1}$ obtained from $MAPbI_3$ single crystal measurements may be strongly influenced by surface or interface effects. However, room temperature mobility values which are estimated to be significantly above 200 $cm^2\ V^{-1}\ s^{-1}$ require careful scrutiny.[65]

We included the polaron parameters of GaAs[57] in Table 2 for comparison. We can attribute the large difference in mobility between GaAs and the perovskites to two material properties: (i) the stronger ionic screening (indicative of a higher ionicity), and (ii) the lower LO phonon energy in the perovskites. The lead halide perovskites are a rare example for semiconductors with a Debye temperature of the LO phonon frequency, $\Omega_D = hc\omega_{LO}/k_B$, below room temperature, leading to a strong occupation of phonon states at 300 K which limits the mobility.

Finally, we briefly discuss the temperature dependence of the carrier mobility. For $MAPbI_3$, a comparison is complicated because the cubic-to-tetragonal phase transition temperature is close to room temperature. For $MAPbBr_3$, the transition occurs around 240 K and so it is generally an easier task. In the ESI† we demonstrate numerically that between 350 K to 250 K the mobility of $MAPbBr_3$, including only the scattering due to optical phonons within the simple model used here, changes as $T^{-0.62}$. Indeed, in contrast to this finding it has been discussed that in the cubic phase the overall temperature dependence of the measured Hall mobility is best described as $T^{-1.4}$,[19] the fingerprint of scattering due to acoustic phonons.[13,16–19] However, several theoretical reports showed that mobilities limited by acoustic phonon scattering should be extremely high,[66,67] which also conflicts with the experimental data. Therefore, we are currently facing the contradiction that, as shown here, the large polaron model provides the incorrect temperature dependence but the correct magnitude of the mobility, and models including scattering only due to acoustic phonons follow the correct temperature dependence but strongly overestimate the mobility itself. This may indicate that one or several assumptions underlying these textbook models of charge-carrier scattering are actually not valid for the case of lead-halide perovskites. Indeed, as we have emphasized throughout this paper, lead-halide perovskites show strongly anharmonic vibrations and dynamic disorder.[8,37–40] Therefore, the canonical picture of charge carriers being scattered by harmonic vibrations of an otherwise rigid ionic lattice may not be valid for lead-halide perovskites. This situation calls for charge-carrier scattering models that do not start from the harmonic approximation and can take the intriguing structural dynamics of lead-halide perovskites fully into account. It also clearly highlights the need for more experimental data to better understand the transport of carriers in lead-halide perovskites.

4 Summary

In summary, we measured and analyzed quantitatively the lattice vibrations of the three methylammonium lead halide perovskites at room temperature. The spectra point to strong anharmonicity and dynamic disorder in these materials at room temperature, similar to certain oxide perovskites.[41] Our detailed analysis of the obtained far IR spectra allows us to directly determine the LO–TO splitting, and deduce the strength of electron–phonon coupling in $MAPbX_3$. Our estimated upper limit for the room temperature mobility in $MAPbI_3$ of ~ 200 cm^2 V^{-1} s^{-1} indicates that there is still considerable room for further improvement of thin film quality, where mobilities of up to 50 cm^2 V^{-1} s^{-1} have been achieved.[7,63] However, we also show that despite only moderate polaron masses, the low LO phonon frequency and high ionicity of the lead halide perovskites fundamentally limit the charge carrier mobilities in these materials.

5 Experimental methods

Thin film preparation

Silicon substrates were cut and cleaned by sonication in acetone and isopropyl alcohol for 10 minutes. Afterwards they were dried in a N_2 stream. For perovskite film preparation we chose a vapor assisted evaporation process. Therefore we used as received $PbCl_2$, $PbBr_2$ (Alfa Aeser) and PbI_2 (Sigma Aldrich) for evaporation. We used a high vacuum chamber with a pressure of 1.5×10^{-5} mbar and evaporated 176 nm thick layers of every one of those three materials at a rate of 8 nm min^{-1}. After evaporation the as evaporated films were transferred into a nitrogen filled glovebox for the vapor assisted process. Accordingly we put the lead halide samples in a petri dish and surrounded it with the corresponding methylammonium halide. We used as received MACl (VWR), MABr, and MAI (DYESOL). For perovskite formation we heated the petri dish for 2 hours at 165 °C, 160 °C and 155 °C respectively. Thus we achieved perovskite films with a layer thickness of approximately 300 nm.

Single crystal preparation

Single crystals of $MAPbCl_3$, $MAPbBr_3$, and $MAPbI_3$ were prepared and characterized using the method described in the literature.[68] In Fig. S5 (ESI†) we show the optical images of the crystals that were used in this study.

IR spectroscopy

The as-fabricated perovskite thin films were transported in nitrogen atmosphere to a Bruker Vertex 80v Fourier transform IR (FTIR) spectrometer and measured under vacuum conditions ($\sim$2 mbar). Spectra were acquired using a liquid Helium cooled Si-Bolometer with unpolarized light and a resolution of 4 cm^{-1}. All spectra were referenced to the bare Silicon substrate with natural oxide at the respective angle of incidence. Spectra of the single crystals were measured in reflectance under an angle of incidence of 80° using unpolarized light and a gold mirror as reference. Scaling of the single crystal spectra was executed due to an improper matching of the focal plane of reference and single crystal.

Optical modeling

Modeling of the measured thin-film spectra was performed using the commercially available software package SCOUT.[69] The used optical model was made of a 1 mm thick Si substrate (described elsewhere[32]) and the $MAPbX_3$ film on top. The film thicknesses of the perovskite layer was determined by mid-infrared FTIR measurement of the same samples and fitting their thin film spectrum with the published optical model.[32] This thickness and the dielectric background ε_∞ was used for

the FIR optical model. The dielectric function of the perovskite thin films furthermore consisted of Gervais oscillators. The resonance frequencies of the transverse and longitudinal optical mode (ω_{TO}, ω_{LO}) and their damping (γ_{TO}, γ_{LO}) were fitted simultaneously for 0° and 70° angle of incidence.

Computational methods

DFT calculations were performed using a cubic unit-cell of $MAPbCl_3$ and a lattice constant of 5.71 Å as previously calculated, see ref. 70 for details. The plane-wave kinetic energy cutoff was set to 400 eV and an 8 × 8 × 8 Γ-centered k-point grid was used for self-consistently calculating the charge-density. The band-structure calculation was performed non-selfconsistently using an equally-spaced k-grid of 100 points ($\Delta k \sim 0.01$ Å^{-1}); the numerical convergence with respect to Δk was verified. To estimate the reduced exciton effective mass, we have fitted the equation, $E(k) = E_0 \pm \frac{\hbar^2 k^2}{m_0 m_{e,h}}$, to the onsets of the valence- and conduction band around R in the direction of Γ in the Brillouin zone, as the fundamental gap occurs at the R-point. The obtained reduced exciton mass is in good agreement with recent GW calculations for $MAPbCl_3$,[56] although individual electron and hole masses show somewhat stronger deviations. This may imply that our estimate for the reduced exaction mass benefits from error cancellation. To test the reliability of our PBE + SOC results, we have also performed HSE + SOC calculations[71,72] on carefully reduced k-grids, from which we obtained a virtually identical reduced exciton mass, similar to what has been reported for $MAPbI_3$ previously.[73]

Acknowledgements

We acknowledge the German Federal Ministry of Education and Research for financial support within the InterPhase project (FKZ 13N13656, 13N13657). The work in Oxford was funded by EPSRC, UK. M. S. and C. M. acknowledge financial support by the Heidelberg Graduate School of Fundamental Physics. P. K. N. is supported by Marie-Curie actions individual fellowships (grant agreement number 653184). D. A. E. and L. K. were supported by the Austrian Science Fund (FWF): J3608-N20 and by a research grant from Dana and Yossie Hollander, in the framework of the WIS Alternative sustainable Energy Initiative.

References

1 W. Zhang, G. E. Eperon and H. J. Snaith, *Nature Energy*, 2016, **1**, 16048.
2 A. Kojima, K. Teshima, Y. Shirai and T. Miyasaka, *J. Am. Chem. Soc.*, 2009, **131**, 6050–6051.
3 M. M. Lee, J. Teuscher, T. Miyasaka, T. N. Murakami and H. J. Snaith, *Science*, 2012, **338**, 643–647.
4 D. B. Mitzi, in *Progress in Inorganic Chemistry*, ed. K. D. Karlin, John Wiley & Sons, Inc., 1999, pp. 1–121.
5 D. Weber, *Zeitschrift für Naturforschung B*, 1978, **33**, 1443.
6 Y. Liu, Z. Yang, D. Cui, X. Ren, J. Sun, X. Liu, J. Zhang, Q. Wei, H. Fan, F. Yu, X. Zhang, C. Zhao and S. F. Liu, *Adv. Mater.*, 2015, **27**, 5176–5183.
7 C. C. Stoumpos, C. D. Malliakas and M. G. Kanatzidis, *Inorg. Chem.*, 2013, **52**, 9019–9038.
8 O. Yaffe, Y. Guo, T. Hull, C. C. Stoumpos, L. Z. Tan, D. A. Egger, F. Zheng, G. Szpak, O. E. Semonin, A. N. Beecher, T. F. Heinz, L. Kronik, A. M. Rappe, M. G. Kanatzidis, J. S. Owen, M. A. Pimenta and L. E. Brus, 2016, arXiv:1604.08107 [cond-mat].
9 D. Shi, V. Adinolfi, R. Comin, M. Yuan, E. Alarousu, A. Buin, Y. Chen, S. Hoogland, A. Rothenberger, K. Katsiev, Y. Losovyj, X. Zhang, P. A. Dowben, O. F. Mohammed, E. H. Sargent and O. M. Bakr, *Science*, 2015, **347**, 519–522.
10 S. D. Stranks, G. E. Eperon, G. Grancini, C. Menelaou, M. J. P. Alcocer, T. Leijtens, L. M. Herz, A. Petrozza and H. J. Snaith, *Science*, 2013, **342**, 341–344.
11 Y. Chen, H. T. Yi, X. Wu, R. Haroldson, Y. N. Gartstein, Y. I. Rodionov, K. S. Tikhonov, A. Zakhidov, X. Y. Zhu and V. Podzorov, *Nat. Commun.*, 2016, **7**, 12253.
12 S. De Wolf, J. Holovsky, S.-J. Moon, P. Löper, B. Niesen, M. Ledinsky, F.-J. Haug, J.-H. Yum and C. Ballif, *J. Phys. Chem. Lett.*, 2014, **5**, 1035–1039.
13 T. M. Brenner, D. A. Egger, A. M. Rappe, L. Kronik, G. Hodes and D. Cahen, *J. Phys. Chem. Lett.*, 2015, **6**, 4754–4757.
14 T. M. Brenner, D. A. Egger, L. Kronik, G. Hodes and D. Cahen, *Nature Reviews Materials*, 2016, **1**, 15007.
15 M. Wang and S. Lin, *Adv. Funct. Mater.*, 2016, **26**, 5297–5306; A. Pisoni, J. Jaćimović, O. S. Barišić, M. Spina, R. Gaál, L. Forró and E. Horváth, *J. Phys. Chem. Lett.*, 2014, **5**, 2488–2492.
16 R. L. Milot, G. E. Eperon, H. J. Snaith, M. B. Johnston and L. M. Herz, *Adv. Funct. Mater.*, 2015, **25**, 6218–6227.
17 H. Oga, A. Saeki, Y. Ogomi, S. Hayase and S. Seki, *J. Am. Chem. Soc.*, 2014, **136**, 13818–13825.
18 T. J. Savenije, C. S. Ponseca, L. Kunneman, M. Abdellah, K. Zheng, Y. Tian, Q. Zhu, S. E. Canton, I. G. Scheblykin, T. Pullerits, A. Yartsev and V. Sundström, *J. Phys. Chem. Lett.*, 2014, **5**, 2189–2194.
19 H. T. Yi, X. Wu, X. Zhu and V. Podzorov, *Adv. Mater.*, 2016, **28**, 6509–6514.
20 C. La-o-vorakiat, H. Xia, J. Kadro, T. Salim, D. Zhao, T. Ahmed, Y. M. Lam, J.-X. Zhu, R. A. Marcus, M.-E. Michel-Beyerle and E. E. M. Chia, *J. Phys. Chem. Lett.*, 2016, **7**, 1–6.
21 E. Menéndez-Proupin, C. L. Beltrán Ríos and P. Wahnón, *Phys. Status Solidi RRL*, 2015, **9**, 559–563.
22 A. D. Wright, C. Verdi, R. L. Milot, G. E. Eperon, M. A. Pérez-Osorio, H. J. Snaith, F. Giustino, M. B. Johnston and L. M. Herz, *Nat. Commun.*, 2016, **7**, 11755.
23 X.-Y. Zhu and V. Podzorov, *J. Phys. Chem. Lett.*, 2015, **6**, 4758–4761.
24 A. J. Neukirch, W. Nie, J.-C. Blancon, K. Appavoo, H. Tsai, M. Y. Sfeir, C. Katan, L. Pedesseau, J. Even, J. J. Crochet, G. Gupta, A. D. Mohite and S. Tretiak, *Nano Lett.*, 2016, **16**, 3809–3816.
25 W. Nie, J.-C. Blancon, A. J. Neukirch, K. Appavoo, H. Tsai, M. Chhowalla, M. A. Alam, M. Y. Sfeir, C. Katan, J. Even,

S. Tretiak, J. J. Crochet, G. Gupta and A. D. Mohite, *Nat. Commun.*, 2016, **7**, 11574.
26 A. M. Soufiani, F. Huang, P. Reece, R. Sheng, A. Ho-Baillie and M. A. Green, *Appl. Phys. Lett.*, 2015, **107**, 231902.
27 Z.-G. Yu, *J. Phys. Chem. Lett.*, 2016, **7**, 3078–3083.
28 F. Brivio, J. M. Frost, J. M. Skelton, A. J. Jackson, O. J. Weber, M. T. Weller, A. R. Goñi, A. M. A. Leguy, P. R. F. Barnes and A. Walsh, *Phys. Rev. B: Condens. Matter Mater. Phys.*, 2015, **92**, 144308.
29 M. A. Pérez-Osorio, R. L. Milot, M. R. Filip, J. B. Patel, L. M. Herz, M. B. Johnston and F. Giustino, *J. Phys. Chem. C*, 2015, **119**, 25703–25718.
30 W. Cochran and R. A. Cowley, *J. Phys. Chem. Solids*, 1962, **23**, 447–450.
31 A. A. Bakulin, O. Selig, H. J. Bakker, Y. L. Rezus, C. Müller, T. Glaser, R. Lovrinčić, Z. Sun, Z. Chen, A. Walsh, J. M. Frost and T. L. C. Jansen, *J. Phys. Chem. Lett.*, 2015, **6**, 3663–3669.
32 T. Glaser, C. Müller, M. Sendner, C. Krekeler, O. E. Semonin, T. D. Hull, O. Yaffe, J. S. Owen, W. Kowalsky, A. Pucci and R. Lovrinčić, *J. Phys. Chem. Lett.*, 2015, **6**, 2913–2918.
33 C. Müller, T. Glaser, M. Plogmeyer, M. Sendner, S. Döring, A. A. Bakulin, C. Brzuska, R. Scheer, M. S. Pshenichnikov, W. Kowalsky, A. Pucci and R. Lovrinčić, *Chem. Mater.*, 2015, **27**, 7835–7841.
34 D. W. Berreman, *Phys. Rev.*, 1963, **130**, 2193–2198.
35 Y. Rakita, S. R. Cohen, N. K. Kedem, G. Hodes and D. Cahen, *MRS Commun.*, 2015, **5**, 623–629.
36 F. Aguado and V. G. Baonza, *Phys. Rev. B: Condens. Matter Mater. Phys.*, 2006, **73**, 024111.
37 A. Poglitsch and D. Weber, *J. Chem. Phys.*, 1987, **87**, 6373–6378.
38 M. T. Weller, O. J. Weber, P. F. Henry, A. M. D. Pumpo and T. C. Hansen, *Chem. Commun.*, 2015, **51**, 4180–4183.
39 J. M. Frost and A. Walsh, *Acc. Chem. Res.*, 2016, **49**, 528–535.
40 D. A. Egger, A. M. Rappe and L. Kronik, *Acc. Chem. Res.*, 2016, **49**, 573–581.
41 T. Ostapchuk, J. Petzelt, V. Zelezny, S. Kamba, V. Bovtun, V. Porokhonskyy, A. Pashkin, P. Kuzel, M. D. Glinchuk, I. P. Bykov, B. Gorshunov and M. Dressel, *J. Phys.: Condens. Matter*, 2001, **13**, 2677.
42 A. M. A. Leguy, J. M. Frost, A. P. McMahon, V. G. Sakai, W. Kochelmann, C. Law, X. Li, F. Foglia, A. Walsh, B. C. O'Regan, J. Nelson, J. T. Cabral and P. R. F. Barnes, *Nat. Commun.*, 2015, **6**, 7124.
43 F. Gervais and B. Piriou, *J. Phys. C: Solid State Phys.*, 1974, **7**, 2374.
44 D. W. Berreman and F. C. Unterwald, *Phys. Rev.*, 1968, **174**, 791–799.
45 H. Rubens and E. F. Nichols, *Ann. Phys.*, 1897, **296**, 418–462.
46 A. Poglitsch and D. Weber, *J. Chem. Phys.*, 1987, **87**, 6373–6378.
47 N. Onoda-Yamamuro, T. Matsuo and H. Suga, *J. Phys. Chem. Solids*, 1990, **51**, 1383–1395.
48 T.-Y. Yang, G. Gregori, N. Pellet, M. Grätzel and J. Maier, *Angew. Chem.*, 2015, **127**, 8016–8021.
49 I. Biaggio, R. W. Hellwarth and J. P. Partanen, *Phys. Rev. Lett.*, 1997, **78**, 891–894.
50 H. Fröhlich, *Adv. Phys.*, 1954, **3**, 325–361.
51 R. W. Hellwarth and I. Biaggio, *Phys. Rev. B: Condens. Matter Mater. Phys.*, 1999, **60**, 299–307.
52 R. P. Feynman, *Phys. Rev.*, 1955, **97**, 660–665.
53 K. Galkowski, A. Mitioglu, A. Miyata, P. Plochocka, O. Portugall, G. E. Eperon, J. T.-W. Wang, T. Stergiopoulos, S. D. Stranks, H. J. Snaith and R. J. Nicholas, *Energy Environ. Sci.*, 2016, **9**, 962–970.
54 G. Kresse and J. Furthmüller, *Phys. Rev. B: Condens. Matter Mater. Phys.*, 1996, **54**, 11169–11186.
55 J. P. Perdew, K. Burke and M. Ernzerhof, *Phys. Rev. Lett.*, 1996, **77**, 3865–3868.
56 M. Bokdam, T. Sander, A. Stroppa, S. Picozzi, D. D. Sarma, C. Franchini and G. Kresse, *Sci. Rep.*, 2016, **6**, 28618.
57 S. Adachi, *J. Appl. Phys.*, 1985, **58**, R1–R29.
58 L. P. Kadanoff, *Phys. Rev.*, 1963, **130**, 1364–1369.
59 J. Feng, *APL Mater.*, 2014, **2**, 081801.
60 R. P. Feynman, R. W. Hellwarth, C. K. Iddings and P. M. Platzman, *Phys. Rev.*, 1962, **127**, 1004–1017.
61 J.-H. Lee, N. C. Bristowe, P. D. Bristowe and A. K. Cheetham, *Chem. Commun.*, 2015, **51**, 6434–6437.
62 I. P. Swainson, C. Stock, S. F. Parker, L. Van Eijck, M. Russina and J. W. Taylor, *Phys. Rev. B: Condens. Matter Mater. Phys.*, 2015, **92**, 100303.
63 C. Wehrenfennig, M. Liu, H. J. Snaith, M. B. Johnston and L. M. Herz, *Energy Environ. Sci.*, 2014, **7**, 2269–2275.
64 Q. Dong, Y. Fang, Y. Shao, P. Mulligan, J. Qiu, L. Cao and J. Huang, *Science*, 2015, **347**, 967–970.
65 D. A. Valverde-Chávez, C. S. Ponseca, C. C. Stoumpos, A. Yartsev, M. G. Kanatzidis, V. Sundström and D. G. Cooke, *Energy Environ. Sci.*, 2015, **8**, 3700–3707.
66 Y. He and G. Galli, *Chem. Mater.*, 2014, **26**, 5394–5400.
67 Y. Wang, Y. Zhang, P. Zhang and W. Zhang, *Phys. Chem. Chem. Phys.*, 2015, **17**, 11516–11520.
68 P. K. Nayak, D. T. Moore, B. Wenger, S. Nayak, A. A. Haghighirad, A. Fineberg, N. K. Noel, O. G. Reid, G. Rumbles, P. Kukura, K. A. Vincent and H. J. Snaith, *Nat. Communs.*, 2016, DOI: 10.1038/ncomms13303.
69 W. Theiss, *Scout*, 2015, http://www.mtheiss.com/.
70 D. A. Egger and L. Kronik, *J. Phys. Chem. Lett.*, 2014, **5**, 2728–2733.
71 J. Heyd, G. E. Scuseria and M. Ernzerhof, *J. Chem. Phys.*, 2003, **118**, 8207.
72 J. Heyd, G. E. Scuseria and M. Ernzerhof, *J. Chem. Phys.*, 2006, **124**, 219906.
73 E. Menéndez-Proupin, P. Palacios, P. Wahnón and J. C. Conesa, *Phys. Rev. B: Condens. Matter Mater. Phys.*, 2014, **90**, 045207.

